No 50

SOCIETY OF AUTOMOTIVE ENGINEERS, INC.
Two Pennsylvania Plaza, New York, N.Y. 10001

Time-Resolved Measurements of Hydrocarbon Mass Flowrate in the Exhaust of a Spark-Ignition Engine

Rodney J. Tabaczynski, John B. Heywood, and James C. Keck
Massachusetts Institute of Technology

SOCIETY OF AUTOMOTIVE ENGINEERS

Automotive Engineering Congress
Detroit, Mich.
January 10–14, 1972

720112

720112

Time-Resolved Measurements of Hydrocarbon Mass Flowrate in the Exhaust of a Spark-Ignition Engine

Rodney J. Tabaczynski, John B. Heywood, and James C. Keck
Massachusetts Institute of Technology

UNBURNED HYDROCARBONS, unlike nitrogen oxides and carbon monoxide, are formed in thin layers on the combustion chamber walls, due to the phenomenon of flame quenching. The flame is extinguished, before it reaches the cold combustion chamber walls, leaving a thin layer of unburned fuel-air mixture. Daniel (1, 2)* was the first to recognize this phenomenon in spark-ignition engines and to show that the quench layers are hydrocarbon rich. Since almost all the hydrocarbons are concentrated in these thin quench regions along the wall, it is expected that boundary layer controls and/or modifications to the combustion chamber could reduce the concentration of hydrocarbons in the exhaust. However, the processes by which the quench layers leave the cylinder have not been investigated. Necessary preliminaries to any control development are experimental data indicating how the various different quench layers leave the cylinder, and their respective contribution to the total hydrocarbons emissions.

Four separate quench regions, whose aerodynamic behavior is expected to be different, are shown in Fig. 1. Region 1 is the head quench layer; region 2, the side wall quench layer; region 3, the piston face quench layer; and region 4, the quench volume between the cylinder wall, piston crown, and first compression ring. When the exhaust valve opens, Fig. 1B, it is expected that the head quench layer, and the part of the side wall quench layer nearest the exhaust valve, will leave the cylinder. The piston face quench layer, on the other hand,

*Numbers in parentheses designate References at end of paper.

ABSTRACT

Experimental measurements of the instantaneous exhaust gas temperature, mass flowrate, and hydrocarbon concentration have been made in the exhaust of a single cylinder research engine. The temperature measurements were accomplished using an infrared optical technique and observing the radiation of the exhaust gas at the 4.4 μm band of CO_2. Instantaneous exhaust gas mass flowrates were monitored by placing a restriction in the exhaust manifold and measuring the instantaneous pressures across the restriction. Time-resolved hydrocarbon concentrations were measured using a fast-acting sampling valve with an open time of 2 ms. From these measurements, the hydrocarbon mass flowrate is calculated as a function of crank angle. The hydrocarbon mass flowrate calculations show that approximately 40% of the hydrocarbons leave the cylinder early in the exhaust process, due to the exit of the head quench layer, and 50% leave the cylinder near the end of the exhaust process, due to the exit of a hydrocarbon-rich vortex produced by the upward motion of the piston. The remainder of the hydrocarbons leave in the middle of the exhaust stroke. The measurements explain why a reduction of the quench volume, created by the clearance between the piston and the first compression ring, reduces average hydrocarbon concentrations.

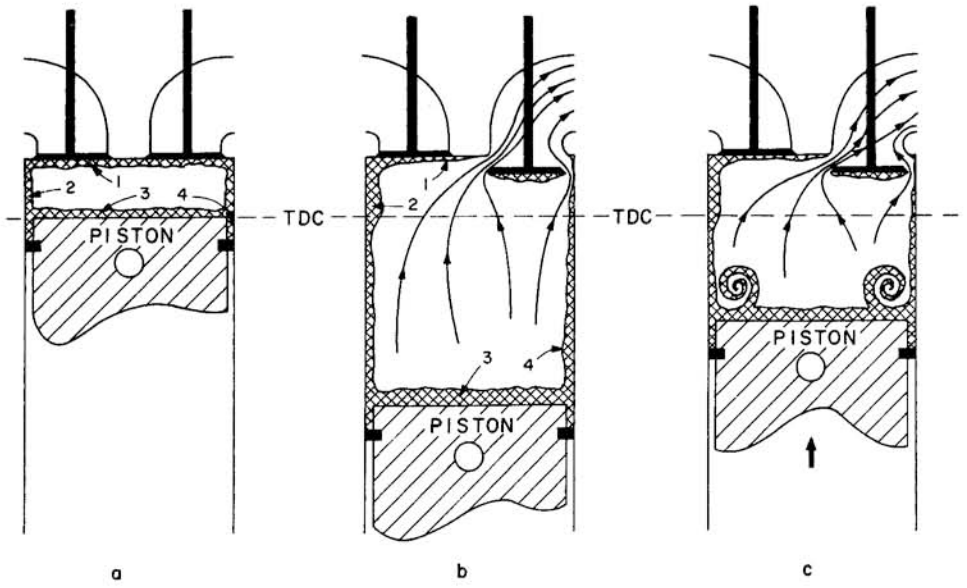

Fig. 1 - (A) Formation of quench layers as flame is extinguished at cool walls. Not to scale, quench layers are about 0.003 in thick. (B) Quench layers have expanded as cylinder pressure falls. Gas in quench volume between piston crown and first ring, 4, has been laid along cylinder wall. Head quench layer, 1 and 2, exits cylinder. (C) Roll-up of hydrocarbon-rich boundary layer into a vortex at piston-cylinder wall interface as piston moves up cylinder

probably will not leave the cylinder at any time in the stroke, since the flow velocities are very small in this region. The motion of the gas adjacent to the cylinder wall could not be determined, since the flow pattern inside the cylinder, as the piston moved upward during the exhaust stroke, was not known.

In a previous experiment, this flow pattern was studied using an incompressible flow model of the exhaust process which simulated typical engine Reynolds numbers (3). The fluid motion as the piston moves upward in the cylinder was studied, using flow visualization techniques, and a vortex flow was observed at the piston cylinder wall interface. A photograph and schematic of this vortex are shown in Fig. 2. Semiempirical theories were developed which correlated measurements of vortex size, stroke, and Reynolds number. These results predict that the vortex is large enough to reach the exhaust valve in an actual engine. The vortex is expected to be rich in hydrocarbons, since, during the expansion stroke as the gas expands, the hydrocarbons from the piston crown-first ring crevice (region 4 in Fig. 1) are laid along the cylinder wall. After the piston reaches bottom dead center, these hydrocarbons are then scraped up by the piston and become part of the vortex. This phenomenon could be an explanation for the occurrence of high hydrocarbon concentrations near the end of the exhaust stroke observed by Daniel (2) (Fig. 2), and for the results of Wentworth (4) which show that a reduction of the piston crown-first ring quench volume substantially reduces average hydrocarbon levels.

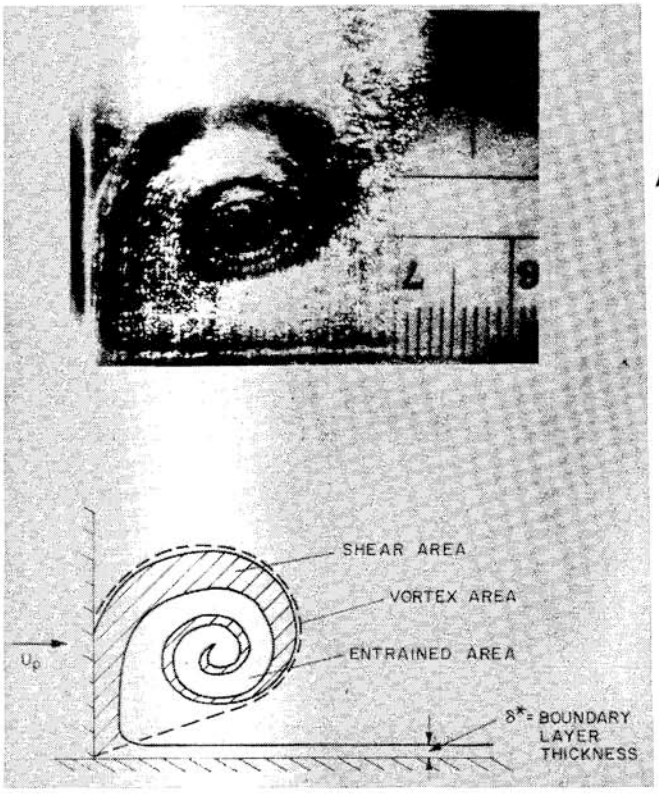

Fig. 2 - Photograph and sketch of vortex flow, piston on left, cylinder wall at bottom

Since Daniel's experiment (2) gave hydrocarbon concentrations in the exhaust as a function of crank angle without corresponding time-resolved mass flowrate measurements, the contributions from the various quench layers to the average hydrocarbon level could not be determined. Therefore, to determine the relative contributions of the vortex mechanism which occur late in the exhaust process, and the quench layers that leave the cylinder early in the exhaust process, an experiment, where the mass flowrate of hydrocarbons was measured as a function of crank angle, has been carried out.

The determination of the time-resolved hydrocarbon mass flowrate requires essentially two measurements. The first measurement involves the determination of the instantaneous exhaust gas mass flowrate. This was accomplished by placing a thick plate orifice in the exhaust manifold and monitoring the instantaneous pressure and temperature upstream of the

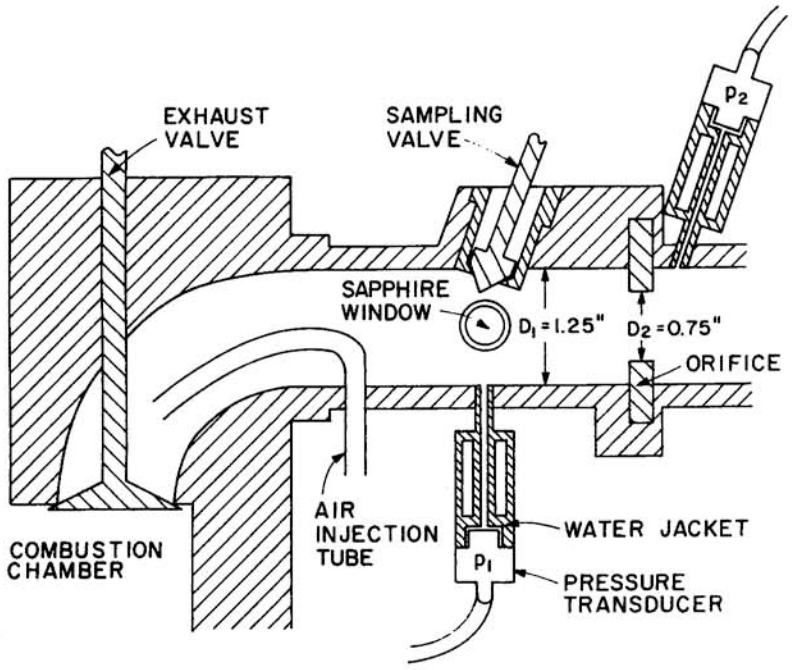

Fig. 3 - Schematic of test section for measurements of exhaust gas temperature, mass flowrate, and hydrocarbon concentration

orifice and the instantaneous pressure immediately downstream of the orifice. A model, which assumes that flow through the orifice is quasi-steady, adiabatic, and isentropic was used to calculate the instantaneous exhaust mass flowrate. The second measurement involved the determination of the time-resolved hydrocarbon concentration in the exhaust manifold. This was accomplished by using a fast-acting sampling valve to extract a sample of exhaust products at various times in the cycle. The volume of gas, between the exhaust valve and sampling station, was purged from cycle to cycle in order to resolve the hydrocarbon concentration in the exhaust just after valve opening. The time-resolved hydrocarbon mass flowrate was then calculated from the formula

$$\dot{m}_{HC} = \dot{m}_E f_{HC} \qquad (1)$$

where:

$\dot{m}_{HC}$ = mass flowrate of hydrocarbons
$\dot{m}_E$ = mass flowrate of exhaust gases
f_{HC} = mass fraction of hydrocarbons

From these results, the relative contributions of the quench layers that leave the cylinder early in the exhaust process, and the vortex mechanism that occurs late in the exhaust process, have been determined.

TIME-RESOLVED EXHAUST GAS MASS FLOWRATE

EXHAUST MASS FLOWRATE MODEL - The exhaust gas mass flowrate was measured as a function of crank angle by placing a restriction (Fig. 3) in the exhaust manifold and assuming that the flow through the restriction was a quasi-steady, adiabatic, and isentropic flow of a perfect gas, modified by a discharge coefficient. The equation governing the mass flowrate for this flow is given in Ref. 5 as

$$\dot{m}_E = C_v A_2 \frac{p_o}{RT_o}\sqrt{\gamma RT_o}\left[\frac{2}{\gamma-1}\left[\left[\frac{p_2}{p_o}\right]^{2/\gamma} - \left[\frac{p_2}{p_o}\right]^{(\gamma+1)/\gamma}\right]\right]^{\frac{1}{2}} \qquad (2)$$

where:

$\dot{m}_E$ = exhaust gas mass flowrate
C_v = discharge coefficient for restriction
A_2 = area of restriction
p_o = stagnation pressure
T_o = stagnation temperature
R = specific gas constant of exhaust gas
γ = ratio of specific heats for exhaust gas
p_2 = static pressure measured at area A_2

From Eq. 2 it is necessary that the three quantities, T_o, p_o, and p_2, be measured as a function of crank angle.

To understand better the mass flowrate measurements obtained using Eq. 2, and measured values of T_o, p_o, and p_2, a first-order model for flow through the exhaust valve was constructed. The flow through the exhaust valve was assumed to be a quasi-steady, adiabatic, and isentropic flow of a perfect gas. The governing equations for this model are given in Ref. 5 as

$$\dot{m}_v = C_v A_v \frac{p_{oc}}{RT_{oc}}\sqrt{\gamma RT_{oc}}\left(\frac{2}{\gamma+1}\right)^{(\gamma+1)/2(\gamma-1)} \qquad (3)$$

Table 1 - Summary of Engine Operating Conditions

Speed	Equivalence Ratio	Airflow, lbm/s	Fuel Flow, lbm/s	Spark Advance, deg btc	Inlet Pressure, psia
1200	0.8	1.1×10^{-2}	5.9×10^{-4}	14	14.31
	0.9	1.1×10^{-2}	6.64×10^{-4}	14	14.31
	1.0	1.1×10^{-2}	7.36×10^{-4}	14	14.31
	1.2	1.1×10^{-2}	8.84×10^{-4}	14	14.31
	1.4	1.1×10^{-2}	10.3×10^{-4}	14	14.31
1500	0.8	1.32×10^{-2}	7.07×10^{-4}	17	14.23
	0.9	1.32×10^{-2}	7.95×10^{-4}	17	14.23
	1.0	1.32×10^{-2}	8.85×10^{-4}	17	14.23
	1.2	1.32×10^{-2}	10.6×10^{-4}	17	14.23
	1.4	1.32×10^{-2}	12.4×10^{-4}	17	14.23
1800	0.8	1.42×10^{-2}	7.62×10^{-4}	20	14.16
	0.9	1.42×10^{-2}	8.56×10^{-4}	20	14.16
	1.0	1.42×10^{-2}	9.51×10^{-4}	20	14.16
	1.2	1.42×10^{-2}	11.4×10^{-4}	20	14.16
	1.4	1.42×10^{-2}	13.3×10^{-4}	20	14.16
2400	0.9	1.54×10^{-2}	9.3×10^{-4}	30	14.03

Note: Exhaust pressure, psia, 14.65; inlet temp., F, 170; oil temp., F, 160; water temp., F, 180; bore, in, 3.25; stroke, in, 4.50; compression ratio, 7.

when

$$p_{oc}/p_E > \left(\frac{\gamma+1}{2}\right)^{\gamma/(\gamma-1)}$$

which is the equation for choked flow. In Eq. 3, $\dot{m}_v$ is the mass flowrate through the valve, C_v is the discharge coefficient, A_v is the area of the valve opening, p_{oc} is the stagnation pressure in the cylinder, T_{oc} is the stagnation temperature in the cylinder, p_E is the exhaust pressure immediately after the valve, and γ and R are as defined previously. For the situation when $p_{oc}/p_c < [(\gamma+1)/2)]^{\gamma/(\gamma-1)}$, the flow is no longer choked and is governed by an equation of the form Eq. 2.

With the knowledge of the initial pressure and mass in the cylinder prior to exhaust valve opening, as well as a knowledge of the exhaust history, these equations, along with the adiabatic relationships, can easily be solved for the mass flowrate through the exhaust valve. The results of the theoretical model for the flow through the exhaust valve will be compared with the measured mass flowrate results later.

EXPERIMENTAL APPARATUS AND TECHNIQUES -

Pressure Measurements - The experiments were conducted on a single-cylinder CFR research engine with a variable compression ratio. All experiments were performed at open throttle at a compression ratio of 7. An unleaded gasoline was used, and the fuel and airflow rates were measured using a rotameter and calibrated standard orifice, respectively. The cylinder pressure was measured using a Kistler piezoelectric transducer model 609, and the crank angle was indicated using an optical slit device. Table 1 shows a summary of operating conditions used in this experiment.

For the calculation of the time-resolved exhaust mass flowrate, a test section (Fig. 3) was designed which allowed for the placement of an orifice in the exhaust manifold approximately 6 in downstream of the exhaust valve. A thick orifice was used, since the exhaust gases were at a high temperature. The physical limitations of the engine prevented placing the orifice and associated measuring devices nearer the exhaust valve. The test section was also equipped with sapphire windows, approximately 5 in from the exhaust valve, so that optical measurements of the temperature could be made. The absolute pressures, p_1 and p_2, across the orifice were monitored, using Statham PA285-TC strain gage transducers. These transducers were water cooled and located approximately 1-1/2 in from the exhaust manifold to prevent attenuation of the pressure pulse. The stagnation pressure, p_o, was obtained by using p_1 as an initial estimate and iterating on the equation for the mass flowrate, Eq. 2, and the Mach number relationships. Typical pressure versus time curves are shown in Fig. 4.

Temperature Measurements - The measurement of the instantaneous exhaust gas temperature was accomplished using an optical technique. A 0.3 m McPherson monochrometer was used to select the wavelength and band pass of the radia-

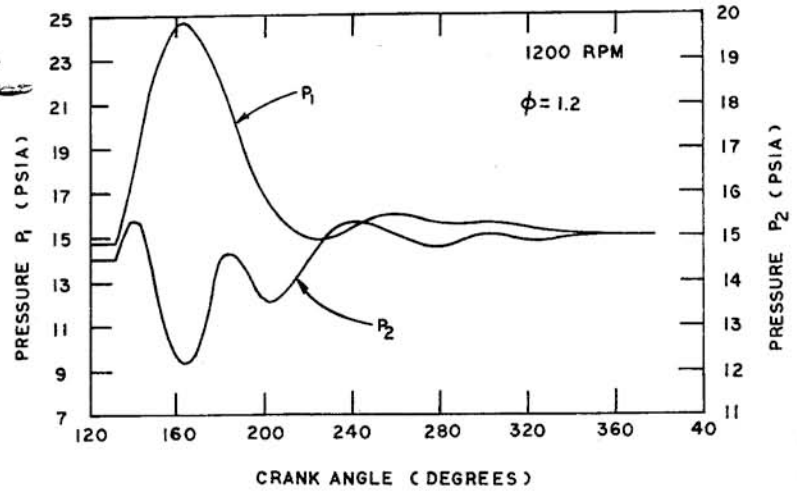

Fig. 4 - Variation of pressures upstream and downstream of orifice, p_1 and p_2, with crank angle for an equivalence ratio of ϕ = 1.2, and an engine speed of 1200 rpm

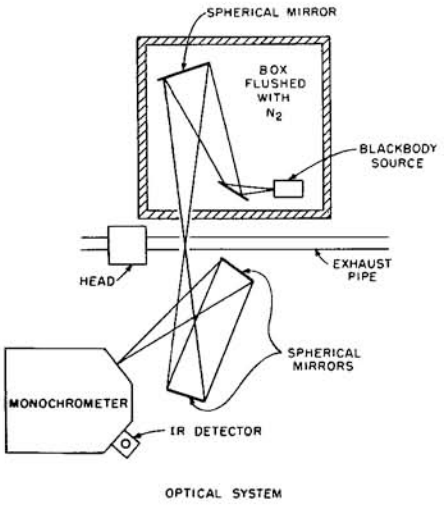

Fig. 5 - Schematic of optical system used for exhaust gas temperature measurement

tion to be studied, as shown in Fig. 5. To make the temperature measurements, the monochrometer was set at 4.4 μm (peak of CO_2 infrared band) with a band pass of 0.09 μm.

The radiation from the exhaust gases was measured with an Indium Antimonide infrared detector. In order to determine the optical thickness of the exhaust gases at 4.4 μm, the two-path technique was utilized (6). By placing a mirror at one end of the field of view (on the outside of the upper window in Fig. 5), the radiation from a doubled-path length can be observed. From the two-path technique, the relationship between the radiation from the two-path lengths is given by:

$$1 - \frac{R^o(\lambda, T_{br2})}{R^o(\lambda, T_{br1})} = - r_\lambda \left[1 - \frac{R^o(\lambda, T_{br1})}{R^o(\lambda, T_E)} \right] \qquad (4)$$

where:

T_{br1} = apparent brightness temperature corresponding to a path length, L

T_{br2} = apparent brightness temperature for 2L

$R^o(\lambda, T_E)$ = blackbody radiancy at true exhaust temperature

r_λ = effective reflectivity of first surface mirror at one end of field of view and contains transmission losses due to windows

Measurements of $R^o(\lambda, T_{br1})$, $R^o(\lambda, T_{br2})$, and r_λ showed that the radiation from the doubled-path length was blackbody radiation. Therefore, all temperature measurements utilized the radiation from the doubled-path length and an emissivity of unity.

A standard blackbody source was used to calibrate the optical system, as shown in Fig. 5, before and after each data run, to ensure that no deterioration of the windows had occurred. An average of ten cycles was recorded, and the radiation curves were very repeatable. The temperature obtained from these measurements is probably close to the average cross-sectional temperature of the exhaust gases. Since the Mach number in the exhaust manifold is generally less than 0.5, the measured temperature was used in place of the stagnation temperature, T_o, for the determination of the mass flowrate.

A theoretical discharge coefficient, C_v = 0.82, (7), was used for the thick orifice plate. This coefficient was checked against a standard orifice under steady flow conditions and agreed within 5%.

DISCUSSION OF RESULTS - Fig. 6 shows the exhaust gas temperature versus crank angle for an equivalence ratio of ϕ = 0.9, and engine speeds 1200, 1500, and 1800 rpm. This figure shows the increase in exhaust gas temperature as the engine speed increases. The increase in exhaust gas temperature occurs since there is less time between cycles for heat transfer to take place; hence, the exhaust manifold temperature and the exhaust gas temperature increase. In Fig. 7, the exhaust gas temperature as a function of crank angle is plotted for an engine speed of 1200 rpm and various equivalence ratios. Note that the exhaust gas temperature decreases as the equivalence ratio varies from unity. This decrease in temperature is

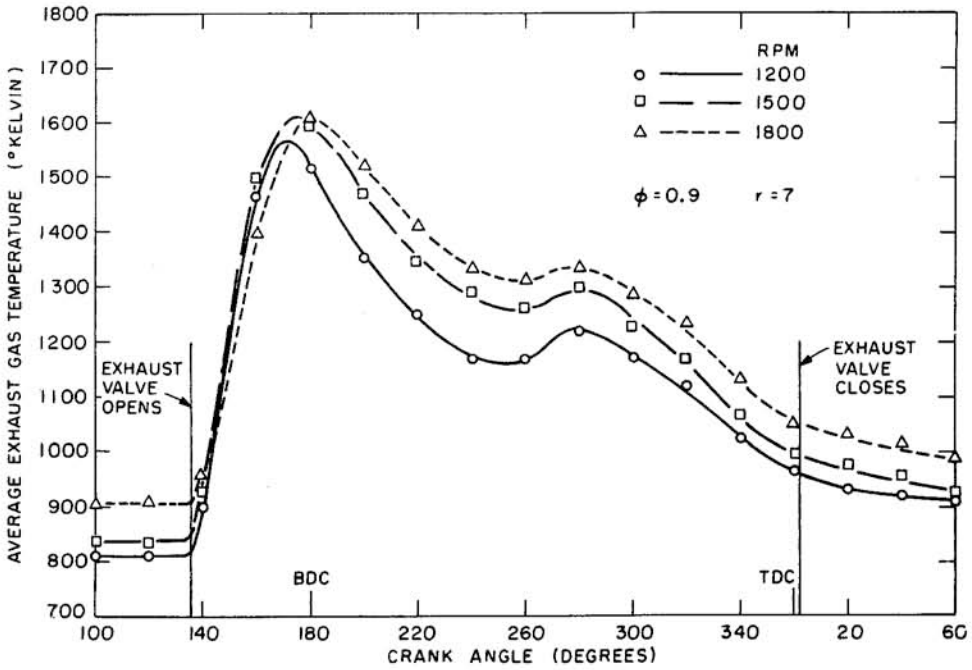

Fig. 6 - Effect of engine speed on average cross-sectional exhaust gas temperature for an equivalence ratio of $\phi = 0.9$

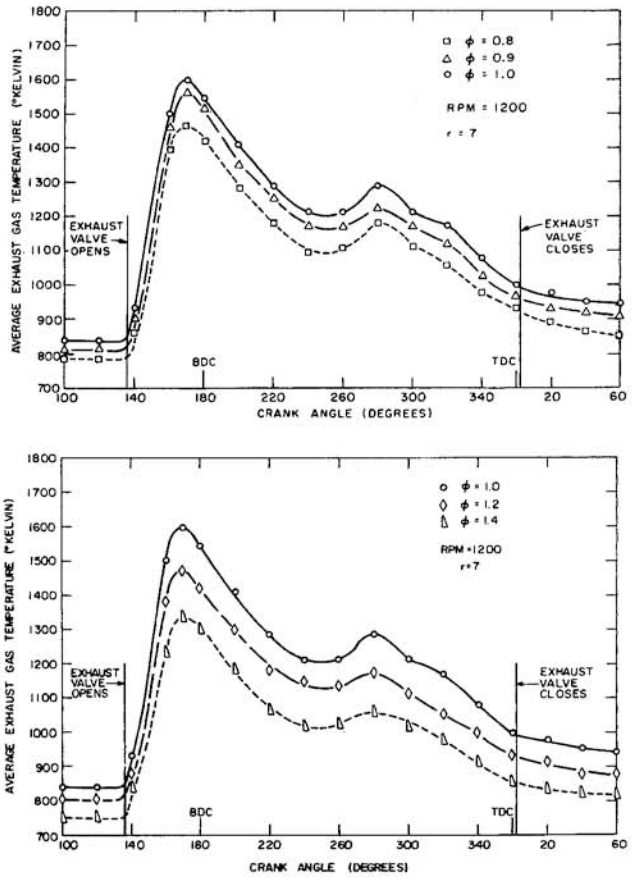

Fig. 7 - Effect of equivalence ratio on average cross-sectional exhaust gas temperature for an engine speed of 1200 rpm

due to the decrease in the adiabatic flame temperatures as the equivalence ratio varies from unity.

Characteristic of all the temperature measurements is the rise in exhaust gas temperature as the exhaust valve opens. This initial flow is cooler due primarily to mixing with the residual gas that was present in the exhaust manifold before the exhaust valve opened. The temperature reaches a maximum at approximately 170 deg crank angle and then decreases as the gas in the cylinder expands. As the piston moves upward, it forces more gas out of the cylinder, and at 270 deg crank angle, a rise in the exhaust gas temperature is observed. At this point, the velocity of the piston reaches a maximum, and the cylinder and exhaust gas pressure rise. Hence, the gas temperature increases. The errors in the temperature measurements are due primarily to uncertainties in mirror reflectivities and the assumption of a gas emissivity of unity. Integrated instantaneous temperatures agreed within 10% of the average exhaust gas temperature measured with a shielded thermocouple.

Fig. 8 shows the exhaust gas mass flowrate as a function of crank angle for an equivalence ratio of $\phi = 1.2$ and engine speeds of 1200, 1500, and 1800 rpm. A characteristic of the mass flow data is the sharp rise in flowrate as the exhaust valve opens, caused by the large pressure differential between the cylinder pressure and exhaust pressure. For typical engine conditions, the pressure ratio, p_c/p_E, causes the flow to be choked for approximately 4.3 ms (30 deg crank angle after valve opening at 1200 rpm). As the cylinder pressure decreases, a point is reached (approximately 170 deg crank angle) where the effect of increasing exhaust valve area is negated by a decreasing cylinder pressure, and the mass flowrate begins to decrease. The flowrate continues to decrease until the effect of the upward motion of the piston becomes important and eventually determines the shape of the mass flowrate curve. The experimental results indicate that a minimum mass flowrate is reached at approximately 220 deg crank angle for 1200 rpm. This minimum point occurs later in the cycle, as engine speed increases, due to the lack of time necessary for the cylinder pressure to equalize with the exhaust

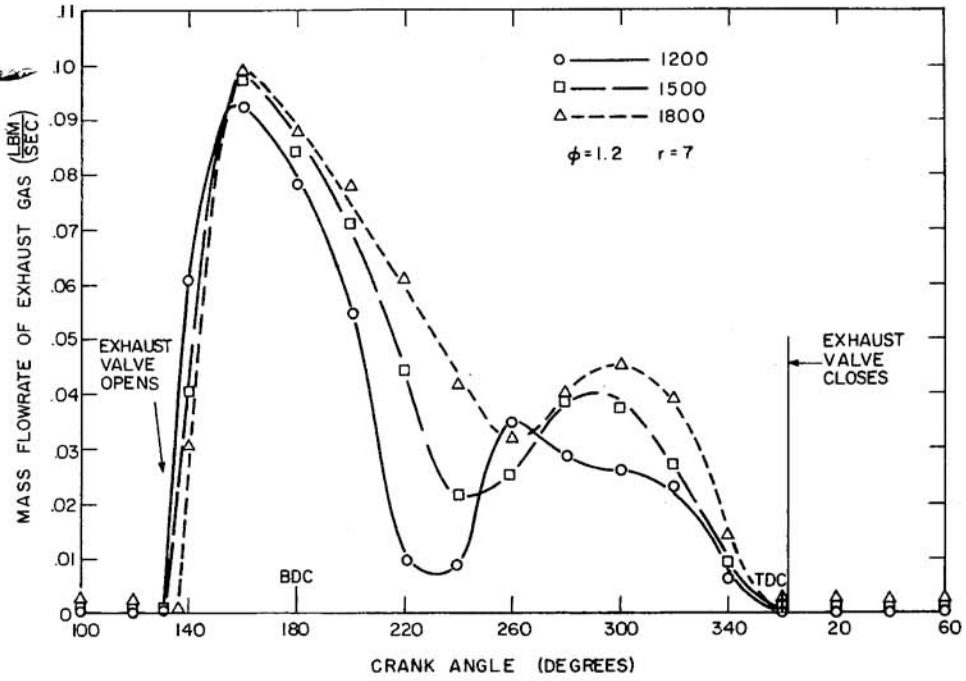

Fig. 8 - Mass flowrate of exhaust gas versus crank angle for an equivalence ratio of $\phi = 1.2$, and engine speeds 1200, 1500, and 1800 rpm

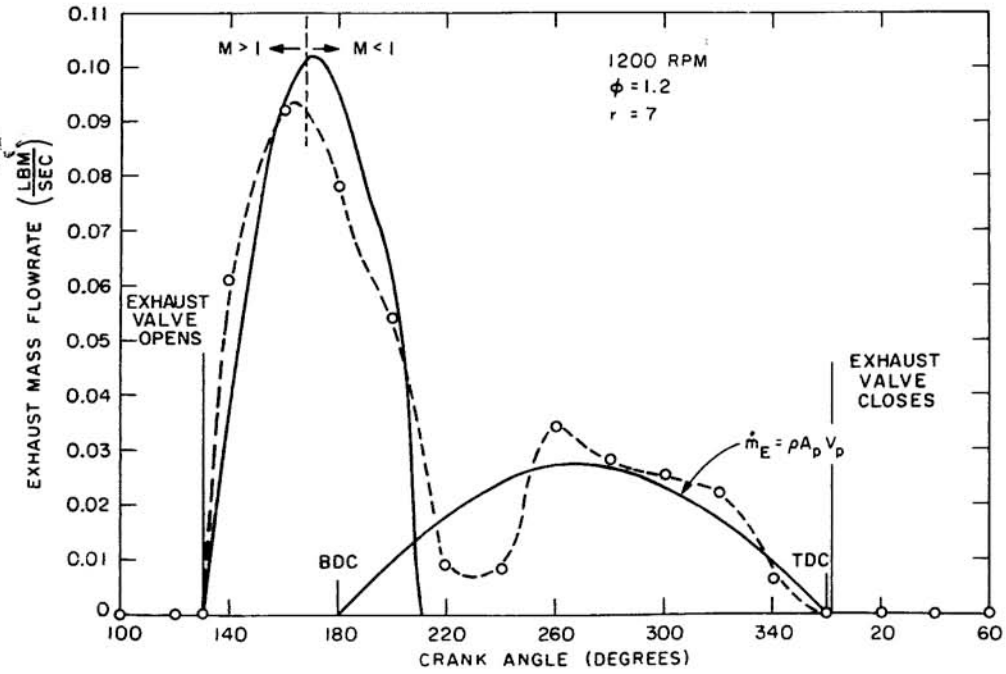

Fig. 9 - Comparison of simple mass flowrate model (solid line) with measured values of mass flowrate for an equivalence ratio of $\phi = 1.2$, and an engine speed of 1200 rpm

pressure before piston movement becomes important. Also, the results show only a slight increase in mass flowrate as the equivalence ratio increases. Integrated instantaneous exhaust mass flow measurements agreed with the average mass flow measurements of air and fuel into the engine to within ±5%.

Figs. 9 and 10 compare the results of the simple model for flow through the exhaust valve with the measured mass flowrate, for an equivalence ratio of $\phi = 1.2$, and engine speeds of 1200 and 1800 rpm, with $\gamma = 1.3$ and R = 55. The model shows the correct shape of the mass flow curve in the region between valve opening and 200 deg crank angle. The effect of piston motion on the mass flowrate was calculated, assuming the gas inside the cylinder was incompressible. This incompressible limit for the mass flowrate is also plotted on these figures, and is in reasonable agreement with the measured mass flowrate near the end of the exhaust stroke. For the case of 1800 rpm and $\phi = 1.2$, the agreement is not as good. However, in the choked flow regime, the general shape of the curve agrees quite well with the measured results. Also, the incompressible limit is in good agreement with the measured values of mass flowrate at the end of the exhaust stroke. It should be pointed out that the model is very sensitive to the rate of opening of the exhaust valve and the pressure differential across the exhaust valve. Note that in Figs. 9 and 10

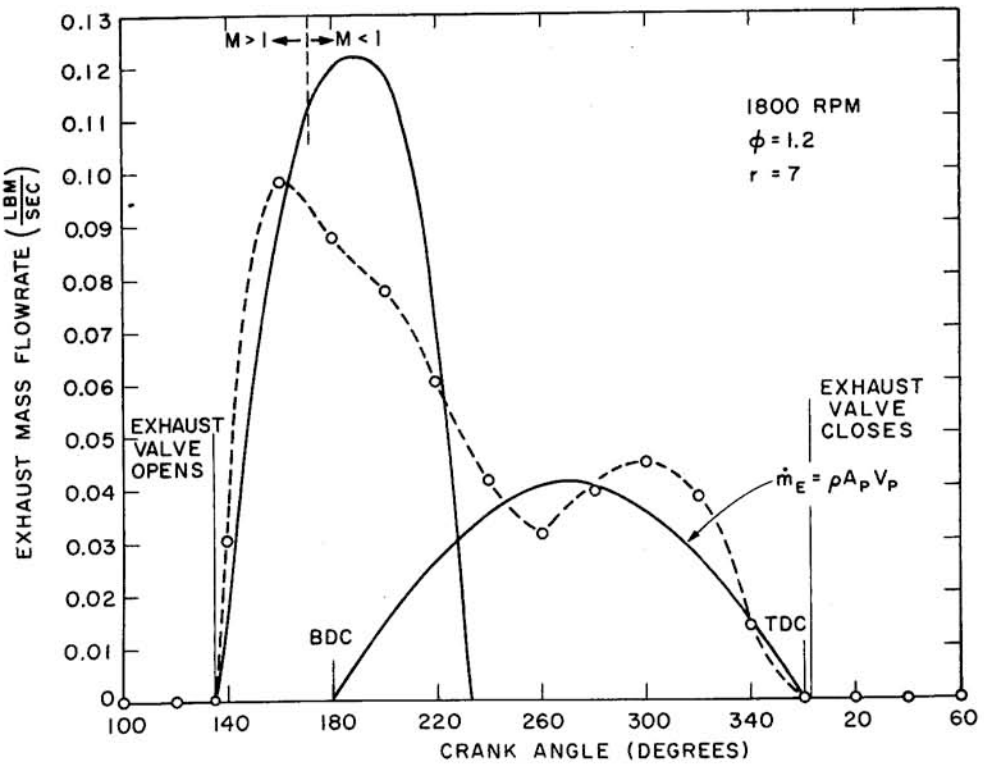

Fig. 10 - Comparison of simple mass flowrate model (solid line) with measured values of mass flowrate for an equivalence ratio of ϕ = 1.2, and an engine speed of 1800 rpm

the measured results imply that the pressure in the cylinder almost equaled that of the exhaust, before the motion of the piston became important, which indicates that the gas in the cylinder overexpanded.

TIME-RESOLVED HYDROCARBON CONCENTRATION AND MASS FLOWRATE

EXPERIMENTAL APPARATUS AND TECHNIQUES - To determine the hydrocarbon concentration as a function of crank angle, an electromagnetically driven, fast-acting sampling valve was used. The sampling valve was placed 5 in downstream of the exhaust valve, as shown in Fig. 3, and could be actuated at any crank angle desired with the use of a light-activated silicon controlled rectifier. The sampling valve has a variable open time of from less than 1 to 3 ms. For use in the exhaust, an open time of 2 ms (14 deg crank angle at 1200 rpm) was selected, so that an adequate sample flowrate could be obtained. Typically, the flowrate was 1200 cm^3/min, which implies that a 6 cm^3 sample at the exhaust gas temperature was extracted from the exhaust each cycle. A detailed report on the design and performance of the sampling valve will be presented in the future. The sampling valve was operated continuously for approximately 5 min (6000 cycles at 1200 rpm) for each measurement. This time could be reduced by shortening the length of the sample line from the valve to the analyzer.

Hydrocarbon concentrations were measured, using a Perkin Elmer Model F11 gas chromatograph equipped with an ionization detector and constant volume gas sample valve. The gas chromatograph was calibrated before, during, and after each data run, and the calibration remained constant to within about 2%. Average hydrocarbon levels were also measured with the same sampling system. The average hydrocarbon levels were sampled from an exhaust mixing tank which had the capacity of approximately ten cylinder volumes. For all concentration measurements, the engine was operated at 1200 rpm, and an equivalence ratio of ϕ = 1.2. Hydrocarbon concentrations are expressed as ppm n-hexane.

It was found that a high hydrocarbon concentration was present in the exhaust after the exhaust valve closes. It was necessary to purge the volume between the exhaust valve and sampling station from cycle to cycle, so that the hydrocarbon concentrations early in the exhaust stroke could be resolved. Fig. 3 shows the placement of the purge tube in the exhaust system. Two different purge rates were used to test the effectiveness of the purge system. An air purge rate of 140 liters/min at S.T.P. was found to be adequate for resolving the early concentrations.

Using the exhaust mass flowrate measurements and the hydrocarbon concentration measurements, the hydrocarbon mass flowrate can be determined from Eq. 1.

DISCUSSION OF RESULTS - Fig. 11 shows hydrocarbon concentration versus crank angle for the cases of no-purge air (dashed line and open squares) and a purge air flowrate of 140 liters/min at S.T.P. (solid line, open, and half-open circles). While the exhaust valve is open, the only appreciable difference between the no-purge and air-purge results occurs during the early part of the exhaust process, between 130 and 160 crank angle degrees. After the exhaust valve closes at tdc, the purge is obviously effective in displacing the stagnant hydrocarbon-rich gas left in the exhaust manifold.

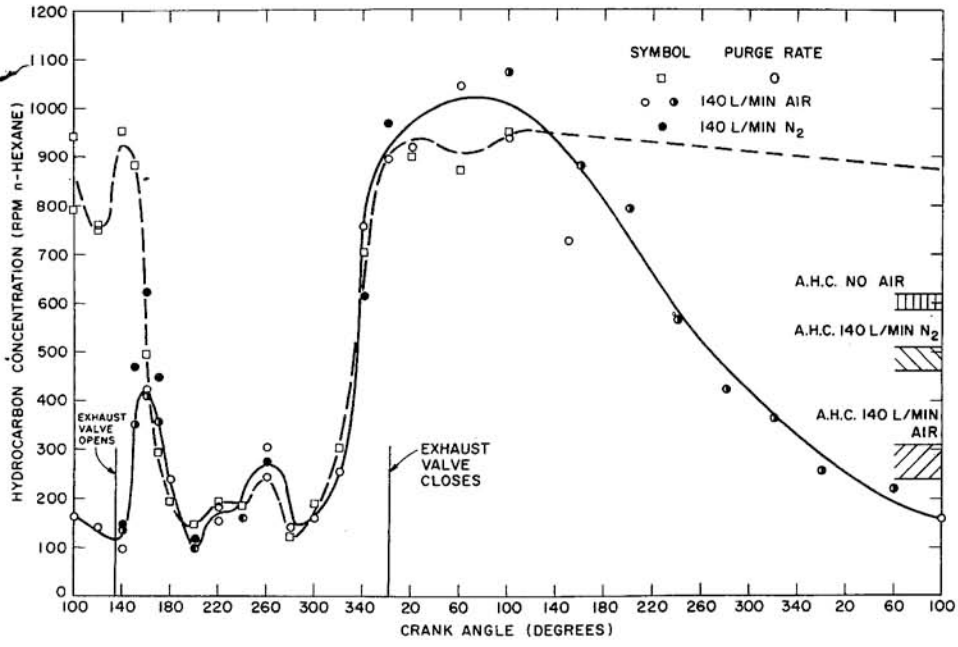

Fig. 11 - Variation of hydrocarbon concentration with crank angle measured at sampling station for purge rates 0 liter/min, 140 liters/min air, and 140 liters/min nitrogen. A.H.C. denotes average hydrocarbon concentration in exhaust flow

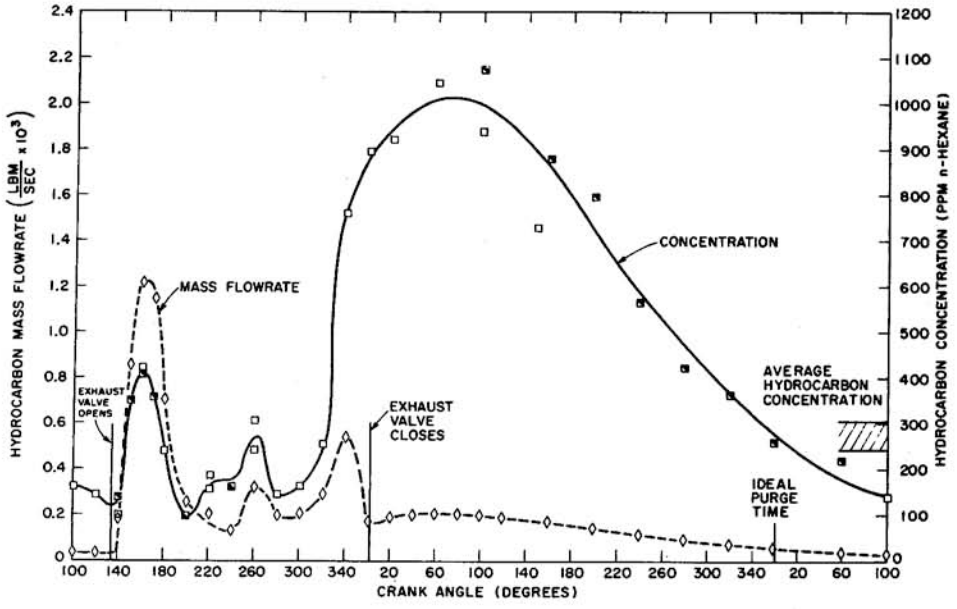

Fig. 12 - Variation of hydrocarbon concentration and hydrocarbon mass flowrate with crank angle measured at sampling station for an air purge rate of 140 liters/min, and equivalence ratio of $\phi = 1.2$, and an engine speed of 1200 rpm

Fig. 11 also shows data points (solid circles) for a nitrogen purge at the same flow rate, 140 liters/min. At the early stages of the exhaust process, the nitrogen purge data points show a higher hydrocarbon concentration than the air purge results—about 50% higher at the peak concentration at 160 deg crank angle. This indicates that there are oxidizing reactions taking place early in the exhaust process where the exhaust gas temperature is highest ($\approx$ 1500 K). Assuming instantaneous mixing between the purge air and exhaust gases at this temperature, and at the oxygen concentration levels present, the correlation developed by Williams, et al. (8) predicts that about 0.2 ms is required for a 30% reduction of methane concentration. Hence, it is expected that significant oxidation of the hydrocarbons will occur, since it takes approximately 1 ms for the exhaust gases to reach the sampling station at the beginning of the exhaust process. However, there is no appreciable difference between the nitrogen purge and air-purge data late in the exhaust process, where the gas temperature is some 300 K lower. The kinetics of Williams, et al. (8) are again consistent with this result, since methane oxidation rates would be orders of magnitude slower at these lower exhaust gas temperatures.

Fig. 11 also shows the average hydrocarbon concentration for the cases of zero, 140 liters/min air, and 140 liters/min N_2 purge rates. The data indicate that the average hydrocarbon concentration for the nitrogen purge is one and one half times that of the air purge, and when allowance is made for the additional gas flow, is approximately equal to the no-purge results. This again points up the importance of oxidizing reactions when an air purge is used.

Fig. 12 shows the hydrocarbon concentrations as a function

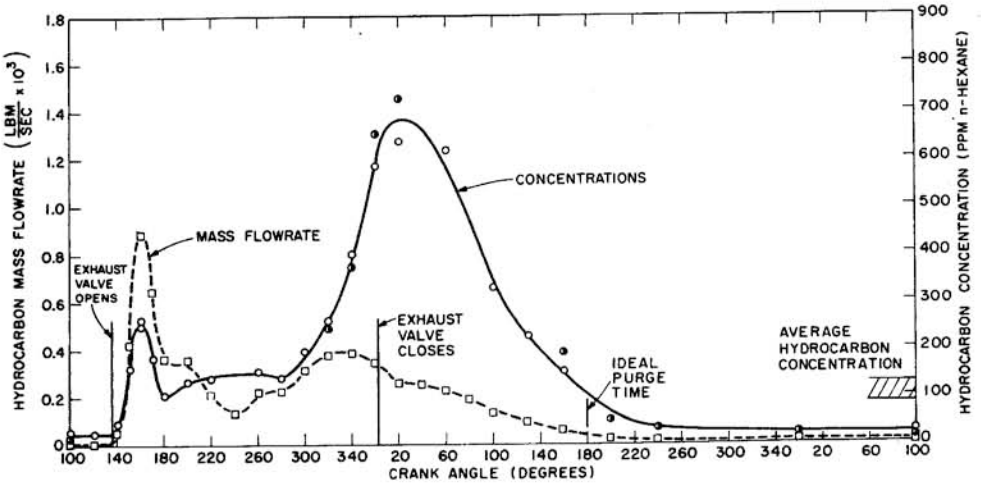

Fig. 13 - Variation of hydrocarbon concentration and hydrocarbon mass flowrate with crank angle measured at sampling station for an air purge rate of 280 liters/min, an equivalence ratio of $\phi = 1.2$, and an engine speed of 1200 rpm

of crank angle for an air purge of 140 liters/min, as well as the hydrocarbon mass flowrate determined using the results of Fig. 8 and Eq. 1. As a result of the air purge, the phenomena occurring at the beginning and end of the exhaust process can be separated. To determine if the purge was operating properly, an air-purge rate of 280 liters/min was used. Fig. 13 shows the hydrocarbon concentration history for the 280 liters/min air purge. The general shape of the concentration profile is similar to the 140 liters/min air purge; however, the hydrocarbon concentration decreases at a faster rate after the exhaust valve closes, due to the increased purge flowrate. Also, the peak hydrocarbon concentration that occurs at 160 deg crank angle is depressed, due to increased oxidizing of the hydrocarbons by the excess oxygen in the purge air. Williams, et al. (8) predict that the oxidation rate is proportional to the square root of the oxygen mass fraction. Hence, doubling the mass flowrate of purge air should decrease the concentration by $1/\sqrt{2}$. This is consistent with the observed results at 160 deg crank angle, and for the average hydrocarbon levels measured.

Figs. 12 and 13 show that, as the exhaust valve opens at 135 deg crank angle, the hydrocarbon mass flowrate increases rapidly due to both an increasing exhaust mass flowrate and increasing hydrocarbon concentration. The hydrocarbon flowrate falls rapidly after 170 deg crank angle, due to a decreasing exhaust mass flowrate and decreasing concentration, until a minimum is reached at 240 deg crank angle. At approximately 300 deg crank angle, the hydrocarbon flow-rate begins to increase until the exhaust valve closes at approximately 360 deg crank ange. A decrease in hydrocarbon flowrate is observed after 360 deg since only the purge air is causing the exhaust gases to flow past the sampling position.

The area under the hydrocarbon mass flow curve, from 135 deg crank angle to about 220 deg crank angle, represents the contribution of the head quench layers and is approximately 40% of the total hydrocarbons. The area under the hydrocarbon mass flowrate curve, from about 300 deg crank angle to exhaust valve opening, is the contribution of the vortex phenomenon to the total hydrocarbon concentration. This area represents approximately 50% of the total hydrocarbon leaving the cylinder. The contribution from the head quench layer

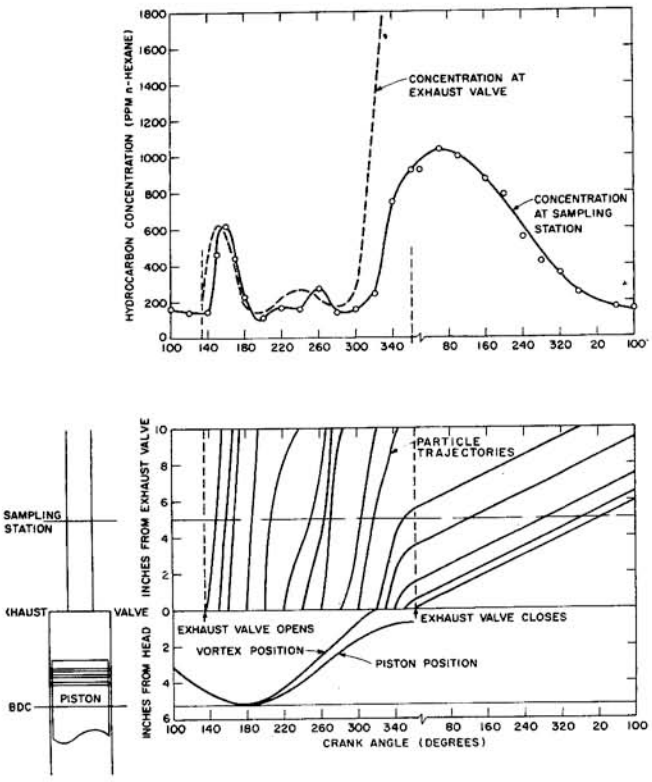

Fig. 14 - A, Hydrocarbon concentration at exhaust valve determined from concentration at sampling station and x-θ diagram; B, x-θ diagram. Upper half shows trajectories of particles leaving cylinder at different crank angles in cycle. Lower half shows piston position and vortex position versus crank angle

is approximately equal to that from the vortex mechanism, if the effects of oxidation are taken into consideration.

It should be noted that Figs. 12 and 13 show hydrocarbon mass flowrates past the sampling valve position. To obtain the flowrate at the exhaust valve, a transformation back to the exhaust valve position has been made. Fig. 14 shows an x-θ plot, indicating piston position, vortex position, and trajectories of particles starting from the exhaust valve at different values of crank angle. The calculation of particle trajectories assumes a plug flow model (that is, all the gas in the exhaust

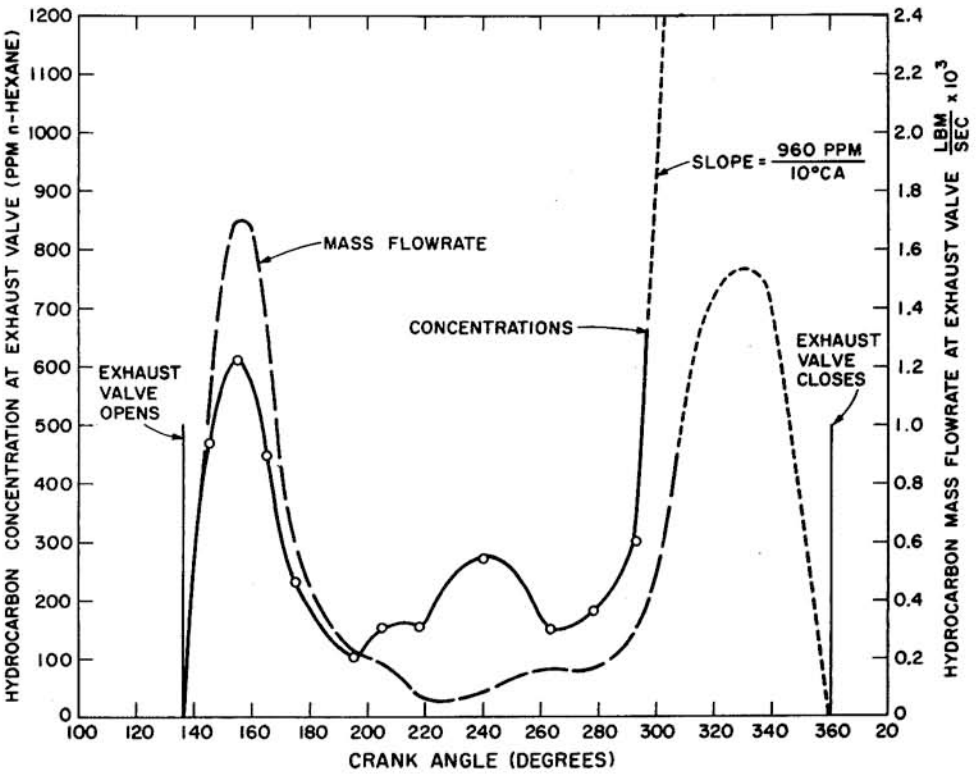

Fig. 15 - Variation of hydrocarbon concentration and hydrocarbon mass flowrate with crank angle at the exhaust valve determined using x-θ diagram of Fig. 14, and experimental results at sampling station

manifold is moving with the same velocity at any instant of time). This is a simple model, designed to shift the concentrations measured at the sampling station to the position of the exhaust valve.

The dashed line in the concentration plot shows the shifted concentration profile. It is expected that the plug flow model will be invalid in two regions. First, at the beginning of the exhaust stroke, when the valve opening is small and the flow through the valve is choked. In this situation, the fluid particles reach the sampling station before the model predicts, since a high velocity jet is emanating from the valve. As the valve opens, one would expect the hydrocarbon concentration to be almost that of the head quench layer. However, in the measurement technique used, a finite sample volume is extracted, and it is impossible to resolve such a high concentration level. The second region where the model is invalid comes at the end of the exhaust stroke. It is not possible to resolve the actual hydrocarbon concentrations in the gas leaving the exhaust valve, because valve lift is small and the velocities through the valve, high. This causes a complicated mixing phenomenon of particles which leave the cylinder at an earlier time with lower velocities and those leaving at a later time with higher velocities.

The lower part of the x-θ plot shows the vortex position as computed from the results of the flow visualization experiment in relation to the piston position. According to the incompressible model, (3) the vortex reaches the exhaust port at 320 deg crank angle; however, the concentration at the exhaust port begins to rise at about 290 deg crank angle, indicating that, for compressible flow, the vortex arrives earlier than predicted. This may be due to the expansion of the vortex ring during the blowdown process as well as a self-propulsion effect due to its high circulation. In any case, the incompressible model can only be applied qualitatively, and the prediction for the arrival time of the vortex is remarkably consistent with the experimental data.

Fig. 15 shows the final results obtained with this transformation. The hydrocarbon concentration and mass flowrate at the exhaust valve location are plotted as a function of crank angle. The hydrocarbon concentration has been corrected for oxidation by using the nitrogen purge results shown in Fig. 11. The shape of the curves at the end of the exhaust process (short-dashed line) was estimated as follows: The area under the hydrocarbon mass flowrate curve, from 290 deg crank angle to exhaust valve closing, must be equal to the area under the hydrocarbon mass flowrate curve, shown in Fig. 12, from 300 deg crank angle to valve opening. It is only necessary, therefore, that the relative shape of the hydrocarbon mass flowrate curve at the valve position be determined. As a first approximation, a linear extrapolation of the concentration profile was assumed. The slope of the extrapolated profile was 96 ppm/-degree crank angle. It should be pointed out that extrapolated concentration values are in agreement with an in-cylinder hydrocarbon concentration of 3700 ppm, sampled at 16 deg btc by Daniel, (2) and the estimate of a hydrocarbon concentration of 5000 ppm in the vortex, assuming that the vortex contains all the quench volume formed by the piston crown and first compression ring (see Appendix). Daniel's result would be expected to be lower, since the sampled gas most likely contained only part of the vortex.

The hydrocarbon mass flowrate curve in Fig. 15 now shows the relative importance of the head quench layer and vortex

mechanism in the total hydrocarbon emissions. The area under the first peak, due to the exit of the head quench layer through the valve, is about 45% of the total hydrocarbon flow. The area under the second peak, at the end of the exhaust process which results from part of the hydrocarbon-rich vortex exiting the valve, is about 55% of the total emissions. These results are in agreement with Wentworth's observation (4) that an 80% reduction in the piston crown-first ring quench volume results in a 40% reduction in average hydrocarbon level. His data add confirmation to the conclusion that the source of the vortex hydrocarbons is this quench volume, and that the vortex is the mechanism by which these hydrocarbons leave the cylinder.

CONCLUSIONS

The hydrocarbon emissions from a spark-ignition engine exit the cylinder in two distinct peaks, one at the start and one at the end of the exhaust process.

The first peak occurs during the blowdown, and is hypothesized to result from entrainment of the cylinder head quench layer.

The second peak occurs as the piston approaches tdc, and results from a vortex motion set up by the piston scraping the hydrocarbon-rich boundary layer from the cylinder wall.

This cylinder-wall hydrocarbon-rich boundary layer is formed as the piston moves down during the expansion stroke, laying the hydrocarbons in the quench volume between the piston crown and first ring along the wall.

The contributions of the head quench layer and the vortex phenomenon to the total hydrocarbon emissions are about equal; for the CFR engine geometry, their respective contributions are 45 and 55%.

Though air injection into the exhaust manifold does reduce total hydrocarbon emissions, only the hydrocarbons that leave the cylinder early in the exhaust process are oxidized.

ACKNOWLEDGMENTS

This work was supported in part by the M.I.T. Sloan Basic Research Fund, the Shell Company's Foundation grant to the Dept. of Mechanical Engineering at M.I.T., and the National Science Foundation, NSF Grant No. GK15409. R. J. Tabaczynski was supported by a Public Health Service Special Air Pollution Fellowship No. 4 FO3 AP 42 339-03 from the National Air Pollution Control Administration.

REFERENCES

1. W. A. Daniel, "Flame Quenching at the Wall of an Internal Combustion Engine." Sixth Symposium (International) on Combustion, Yale University, New Haven, Conn. New York: Reinhold Publishing Co., 1956.

2. W. A. Daniel and J. T. Wentworth, "Exhaust Gas Hydrocarbons-Genesis and Exodus." SAE Technical Progress Series, Vol. 6, "Vehicle Emissions." New York: Society of Automotive Engineers, Inc., 1964.

3. R. J. Tabaczynski, D. P. Hoult, and J. C. Keck, "High Reynolds Number Flow in a Moving Corner." J. Fluid Mechanics, Vol. 42 (June 1970), pp. 249-255.

4. J. T. Wentworth, "Piston and Ring Variables Affect Exhaust Hydrocarbon Emissions." SAE Transactions, Vol. 77 (1969), paper 680109.

5. J. A. Owczarek, "Fundamentals of Gas Dynamics." Scranton, Penn.: International Textbook Co. (1964), pp. 204-205.

6. S. S. Penner, "Quantitative Molecular Spectroscopy and Gas Emissivities." Reading, Mass.: Addison-Wesley, 1959.

7. R. S. Sabersky and A. J. Acosta, "Fluid Flow - A First Course in Fluid Mechanics." New York: MacMillan Co. (1964), p. 86.

8. G. C. Williams, H. C. Hottel, and A. C. Morgan, "The Combustion of Methane in a Jet-Mixed Reactor." Twelfth Symposium (International) on Combustion, The Combustion Inst. (1965), pp. 913-925.

APPENDIX

DETERMINATION OF HYDROCARBON CONCENTRATION IN VORTEX

Since most of the quench volume between the piston face and first ring is laid along the cylinder wall during the expansion stroke, and subsequently scraped up into the vortex during the exhaust stroke, it is possible to make an estimate of the concentration of hydrocarbons in the vortex (3) (Figs. 1 and 2). It will be assumed all of the quenched hydrocarbon from the piston crown-first ring crevice is contained in the vortex. The geometry of the CFR piston and cylinder wall is shown in Fig. A-1. The quench volume during combustion is equal to the volume of the crevice, which is $V_i = 0.046$ in^3 at 400 psia. Since we are interested in this volume after the cylinder pressure becomes atmospheric, it is necessary to determine the volume of this region at 15 psia. If the expansion process is isothermal, the final volume is 1.22 in^3.

The volume of the vortex can be calculated from Fig. A-2 (3) and, for a typical engine Reynolds number $UX/\upsilon = 2 \times 10^3$, the vortex volume is

$$V_v = \pi D_p A = \pi\, 3.25(40 \times 10^{-2}) = 4.1 \text{ in}^3 \quad \text{(A-1)}$$

where:

D_p = diameter of piston

A = area of vortex

The hydrocarbon concentration in the vortex can then be calculated from the formula

$$[HC]_v = (V_i/V_v)\,[HC]_q \quad \text{(A-2)}$$

If the gas in the quench layer is pure fuel-air vapor, the concentration can be calculated from the mole fraction of hydrocarbons in the unburnt fuel-air mixture. For isooctane, the concentration of hydrocarbons is 1.66×10^4 ppm as n-hexane. The concentration of hydrocarbons in the vortex is thus about 5000 ppm, which is the same order of magnitude as the concentration observed by Daniel (2) inside the engine cylinder near the end of the exhaust stroke.

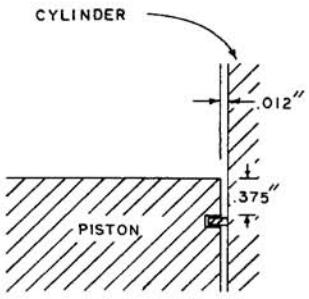

Fig. A-1 - Schematic of piston crown-first ring quench volume in CFR engine

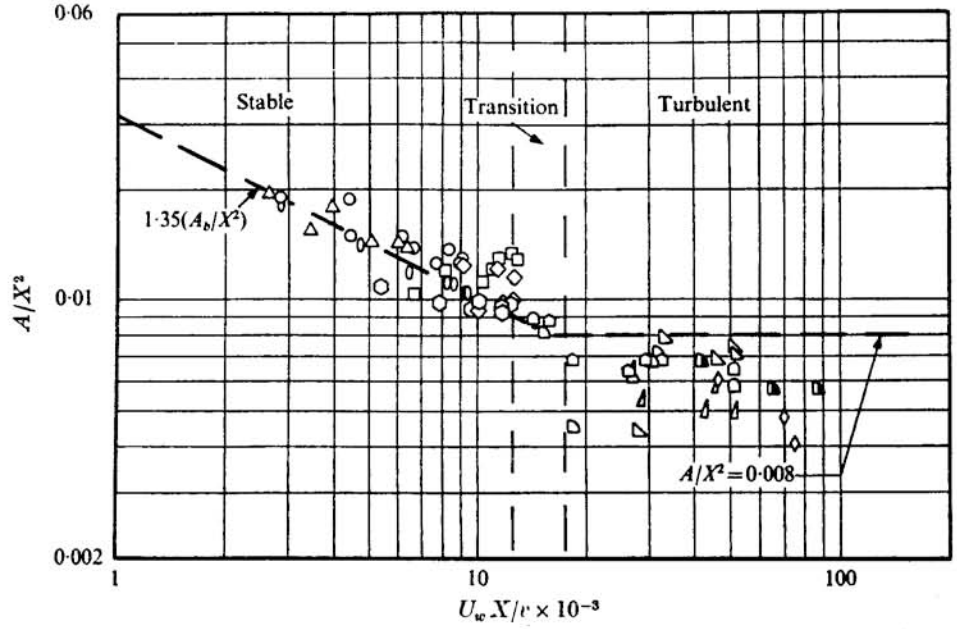

Fig. A-2 - Ratio of vortex area to stroke squared versus Reynolds number for sinusoidal wall velocities